ISSN: 2472-3703 DOI: 10.6911/WSRJ.202603_12(3).0006

Study on the Flow Field Characteristics of a Gas–Liquid–Solid Three-Phase Combined Impeller Agitator Based on CFD

Wenlong Yang *

School of Mechanical Engineering, Xi'an Shiyou University, China

* Corresponding author

Abstract

To address the issues of mixing efficiency and impeller configuration in the gas–liquid–solid three-phase system during CO_2 mineralization and sequestration using coal-based solid waste, a numerical investigation of the internal flow characteristics in a three-phase stirred reactor was carried out using computational fluid dynamics (CFD). A reactor model was established using Fluent simulation software. The multiple reference frame (MRF) method was adopted to construct the stirring flow-field model, and the Navier–Stokes equations were employed as the governing equations. The standard k–ε turbulence model was applied to solve the fluid flow in the stirred tank. Under a stirring speed of 100 r/min, the flow-field characteristics of different impeller combination schemes were simulated and analyzed. By examining the axial, radial, and tangential velocity distributions at specific cross-sections of the reactor, and combining velocity contours with the distributions of solid volume fraction and gas volume fraction, the flow characteristics and mixing performance of different impeller combinations were comparatively studied. The results show that different impeller combinations have significant effects on the internal flow-field structure and multiphase distribution in the reactor. Among the investigated configurations, the combination of an upper double-helical ribbon impeller and a lower pitched-blade turbine impeller can generate a more pronounced axial circulation flow, promoting the suspension of solid particles and the dispersion of gas bubbles. This configuration results in a more uniform distribution of the three phases within the reactor and improves the overall mixing efficiency of the system. The findings provide a theoretical reference for the structural optimization of three-phase stirred reactors and the design of impeller combinations in the CO_2 mineralization and sequestration process using coal-based solid waste.

Keywords

Double helical ribbon and three-pitched blade turbine combined impeller; Gas–liquid–solid three-phase agitator; Multiple reference frame (MRF); Numerical simulation.

1. INTRODUCTION

Carbon dioxide mineralization sequestration technology is considered a carbon storage approach with long-term stability. In 1990, Willy Seifritz [1] first proposed the concept of permanently storing greenhouse gases by reacting silicate minerals with CO_2 to form stable carbonates. This technology has since been regarded as one of the important approaches for long-term CO_2 storage.

This technology utilizes minerals or industrial solid wastes rich in alkaline metals such as calcium and magnesium in nature, which react with CO_2 through carbonation reactions to form stable carbonate minerals, thereby achieving the permanent sequestration of CO_2. Because the

ISSN: 2472-3703 DOI: 10.6911/WSRJ.202603_12(3).0006

resulting carbonates are thermodynamically stable and can persist over long periods, mineralization sequestration is considered a safe and reliable method for carbon storage.

At present, CO_2 mineralization mainly involves two technical routes: direct carbonation and indirect carbonation. Direct mineralization refers to the process in which mineral raw materials react directly with CO_2 to form carbonates without undergoing complex pretreatment. In contrast, indirect mineralization involves preliminary steps such as mineral dissolution and ion extraction, followed by the carbonation reaction [2].

In the direct mineralization process, the reaction can be further classified into dry carbonation and wet carbonation according to the reaction system [3-6]. Dry carbonation [7, 8] is mainly a gas–solid reaction process in which CO_2 directly reacts with mineral feedstock to form metal carbonates. However, this method generally requires relatively high temperature and pressure conditions, and its CO_2 utilization efficiency and fixation capacity are comparatively low. In contrast, wet carbonation [9, 10] involves dissolving CO_2 in water to form a carbonic acid system, in which the ions in solution react with Ca^{2+}, Mg^{2+}, and other ions released from mineral dissolution to form carbonate precipitates. This method operates under relatively mild reaction conditions and can effectively improve the reaction rate and mineralization efficiency; therefore, it has attracted considerable attention in engineering applications. However, the mineralization process usually involves complex interactions among CO_2 gas, liquid phases, and solid mineral feedstocks. Consequently, efficient mixing and mass transfer processes play a crucial role in improving the overall mineralization reaction efficiency.

Against this background, gas–liquid–solid three-phase stirred reactors have gradually become an important type of equipment for CO_2 mineralization reactions. Stirred reactors can enhance internal circulation within the system through mechanical agitation, thereby promoting gas dispersion, solid suspension, and multiphase mass transfer, which improves the overall reaction efficiency. Previous studies have shown [11] that factors such as impeller configuration, rotational speed, and installation position can significantly influence the internal flow-field structure and multiphase distribution characteristics within the reactor.

Meanwhile, computational fluid dynamics (CFD) has become an effective tool for investigating the flow characteristics of three-phase stirred reactors. Xu et al. [11] conducted numerical simulations of gas–liquid–solid three-phase flow in a stirred reactor by establishing an Eulerian multiphase model combined with the k–ε turbulence model, thereby analyzing the suspension behavior of solid particles and the gas dispersion characteristics under different stirring conditions.

Brucato et al. [12] compared experimental data from stirred reactors equipped with single-layer and double-layer impellers with numerical simulation results obtained using the sliding mesh method. The results showed that the sliding mesh approach can accurately characterize the internal flow-field characteristics of stirred reactors. Guozhong Zhou [13] also applied the sliding mesh method to calculate the flow field in a Rushton turbine stirred tank, and the simulation results showed good agreement with experimental data.

In this study, the sliding mesh method was adopted to establish a CFD model of an industrial-scale gas–liquid–solid three-phase stirred reactor. Under identical operating conditions, reactor dimensions, stirring speeds, and gas flow rates, the effects of different combined impeller configurations on the internal flow field of the stirred reactor and the distribution characteristics of the gas–liquid–solid three phases were investigated.

ISSN: 2472-3703 DOI: 10.6911/WSRJ.202603_12(3).0006

2. MATHEMATICAL MODEL AND BOUNDARY CONDITIONS

2.1. Governing Equations

The Navier–Stokes equations are the fundamental constitutive equations used to describe fluid flow problems, which are mainly based on the principles of mass conservation, energy conservation, and momentum conservation. The general basic form of the governing equations is expressed as follows:

The continuity equation represents the law of mass conservation, which states that the rate of change of fluid mass within a control volume is equal to the difference between the mass flow entering and leaving the system [14]. The specific equation is expressed as follows:

$$\frac{\partial \rho}{\partial t} + \nabla \cdot (\rho \vec{v}) = 0 \tag{1}$$

The momentum conservation equation describes that the rate of change of momentum of a fluid element is equal to the resultant external force acting on it, which represents the application of Newton's second law in fluid mechanics. The resultant force includes both body forces and surface forces. The equation is expressed as follows:

$$\rho\left(\frac{\partial u}{\partial t} + u\frac{\partial u}{\partial x} + v\frac{\partial u}{\partial y} + w\frac{\partial u}{\partial z}\right) = \rho f_x + \frac{\partial \sigma_{xx}}{\partial x} + \frac{\partial \tau_{yx}}{\partial y} + \frac{\partial \tau_{zx}}{\partial z} \tag{2}$$

The energy conservation equation states that the rate of change of internal energy of the fluid within a control volume per unit time is equal to the sum of the heat generation rate, the heat increase caused by thermal conduction, and the heat generated by viscous dissipation. This equation follows the law of energy conservation [15]. The expression is given as follows:

$$\frac{\partial (\rho E)}{\partial t} + \nabla \cdot (\rho E \mathbf{v}) = -\nabla \cdot \mathbf{q} + \nabla \cdot (\tau \cdot \mathbf{v}) + \rho \mathbf{v} \cdot \mathbf{f} + \dot{Q} \tag{3}$$

2.2. Numerical Method

The Multiple Reference Frame (MRF) method is a steady-state numerical approach commonly used in the simulation of stirred equipment. In this method, the computational domain is divided into two regions: a rotating region and a stationary region. In the rotating region, the governing equations are solved in a rotating reference frame, whereas in the stationary region they are solved in an inertial reference frame. The two regions are coupled through an interface where physical quantities such as velocity are maintained continuously, enabling the transfer of information between the rotating flow field and the stationary flow field. To ensure the accuracy of the simulation results, the interface between the rotating and stationary regions should be selected carefully so as to minimize its influence on the overall flow-field structure [16].

The MRF method describes the influence of impeller rotation on the flow field by introducing a rotating reference frame in the rotating region without changing the mesh structure. Therefore, this method does not require dynamic mesh updating, avoiding the computational complexity associated with the continuous mesh updating required in the sliding mesh method during the calculation process. As a result, it offers advantages such as good computational stability and relatively low computational cost, and has become one of the most widely used methods for numerical simulation of flow fields in stirred systems [12].

ISSN: 2472-3703 DOI: 10.6911/WSRJ.202603_12(3).0006

3. IMPELLER STRUCTURE DIMENSIONS AND CALCULATION PARAMETERS

3.1. Three Combined Impeller Configurations

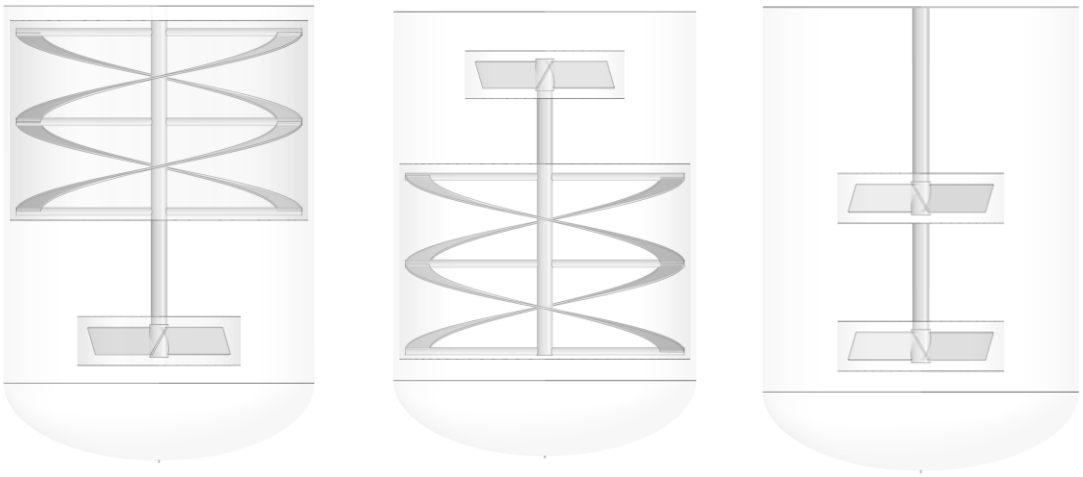
First, a three-dimensional geometric model of the stirred reactor was established in SolidWorks, and the model was then imported into ANSYS for preprocessing. The computational domain was discretized using an unstructured mesh, and local mesh refinement was applied near the upper and lower impellers as well as at the gas inlet to improve the computational accuracy in regions with complex flow behavior. The specific dimensional data of the impeller structure are shown in Table 1.

To investigate the effects of different stirring structures on the internal flow field and multiphase distribution characteristics within the reactor, three typical impeller configurations were selected for numerical simulation in this study, as shown in Figure 1. Scheme 1 consists of a combined configuration of an upper helical ribbon impeller and a lower turbine impeller. In this arrangement, the upper helical ribbon impeller generates a strong axial circulation flow, while the lower turbine impeller produces a radial jet and enhances local turbulence. This configuration facilitates gas dispersion at the bottom of the reactor and strengthens the overall circulation flow.

Scheme 2 consists of a combined configuration of an upper turbine impeller and a lower helical ribbon impeller. In this arrangement, the lower helical ribbon impeller enhances the axial transport capacity in the bottom region, enabling solid particles to be more easily entrained into the main circulation zone. Meanwhile, the upper turbine impeller further strengthens local shear effects and promotes gas dispersion.

Scheme 3 consists of a double-layer turbine impeller configuration. This structure is dominated by radial jet flow and exhibits strong local shear effects and relatively high turbulent kinetic energy, and can therefore serve as a typical radial-flow stirring configuration for comparison.

By comparatively analyzing the flow-field characteristics and multiphase distribution patterns of the three stirring configurations described above, the roles of axial circulation flow and radial jet flow in the gas–liquid–solid three-phase system can be further elucidated, thereby providing a reference for the optimization of stirring structures.



Scheme1 Scheme2 Scheme3

Figure 1. Structural diagrams of three combined impeller configurations

ISSN: 2472-3703 DOI: 10.6911/WSRJ.202603_12(3).0006

Table 1. Specific structural parameters of the agitator

Geometric parameter	Value
Stirred tank diameter, D/mm	1900
Outer diameter of helical ribbon impeller, d/mm	1750
Pitch of helical ribbon, p/mm	1100
Thickness of helical ribbon, s/mm	10
Width of helical ribbon, w/mm	150
Shaft diameter ds/mm	100
Agitator height, H/mm	2800
Pitched blade impeller diameter, Ds/mm	950
Blade width, Ws/mm	190
Blade angle, θ/°	30
Number of blades, Ns/mm	3
Impeller bottom clearance, Hj/mm	630
Impeller spacing, L	890

3.2. Boundary Condition Settings

When the Multiple Reference Frame (MRF) method is used for numerical simulation, the computational domain must be divided into a rotating region and a stationary region according to the impeller structure. The region containing the impeller blades and the surrounding fluid is defined as the rotating domain to describe the influence of impeller rotation on the local flow field, while the main body of the stirred tank and the fluid regions far from the impeller are defined as the stationary domain. The interface between the rotating and stationary domains is set as an Interface, through which the transfer and coupling of physical quantities between the two regions are achieved. This ensures the continuity of parameters such as velocity and pressure at the interface, thereby enabling information exchange between the rotating flow field and the stationary flow field [16]. Figure 2 shows the division method of the rotating and stationary domains for Scheme 1.

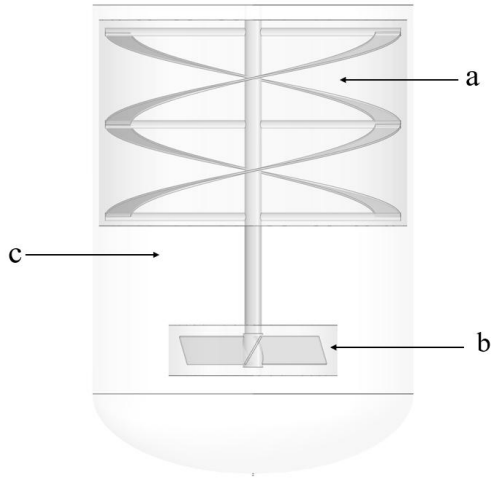
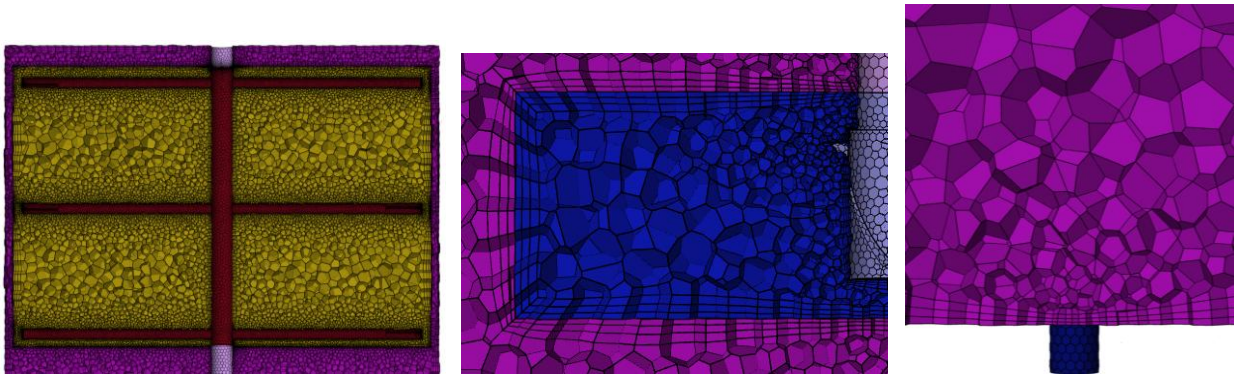


Figure 2. Division of rotating and stationary regions (a: rotating region 1; b: rotating region 2; c: stationary region)

To ensure the accuracy of the simulation results, the stirred reactor model was discretized using a mesh generation process. The overall computational domain was discretized with an unstructured mesh, and local mesh refinement was applied in geometrically complex regions such as the impellers and tank walls to improve the ability to capture detailed flow-field characteristics, as shown in Figure 3 (a) Meanwhile, boundary layer meshes were generated

ISSN: 2472-3703 DOI: 10.6911/WSRJ.202603_12(3).0006

near the solid walls, as illustrated in Figure 3 (b) and Figure 3 (c), to better describe the velocity gradient variations in the near-wall region, thereby improving the stability and accuracy of the numerical calculations. By appropriately controlling the mesh number and mesh quality, computational efficiency was maintained while ensuring sufficient calculation accuracy.



(a) Local mesh refinement near the helical ribbon impeller (b) Boundary layer mesh near the turbine impeller (c) Outlet mesh

Figure 3. Local mesh refinement and boundary layers

3.3. Computational Parameters

The working medium in the simulation was a gas–liquid–solid three-phase system. The gas phase was CO_2, which was introduced through a single gas inlet located at the bottom of the reactor. The diameter of the gas inlet was 10 mm, and the gas inlet velocity was set to 3.5 m/s.

The liquid phase was water, which provided the reaction and mass transfer environment. The solid phase consisted of mixed particles of fly ash and cement, which were dispersed in the liquid phase through agitation. The equivalent density of the solid phase was set to 2306 kg/m^3, and the dynamic viscosity was 0.3 Pa·s.

4. ANALYSIS OF SIMULATION RESULTS

4.1. Flow Field Structure Analysis

Figure 4 shows the velocity distribution contours of the three impeller configurations on the vertical plane. From the overall distribution characteristics, it can be seen that the solid-phase velocity distribution formed by different impeller types differs significantly.

Figure 4 (a) shows that near the upper double helical ribbon impeller of Scheme 1, there is a distinct medium-to-high velocity region. The helical ribbon primarily drives the fluid in the axial direction, and a noticeable velocity band appears near the tank wall, indicating that the fluid flows upward along the wall under the action of the ribbon. Near the lower pitched-blade turbine impeller, local medium-to-high velocity regions are observed. This impeller generates radial jets during rotation, along with some axial components. As shown in Figure 4 (d), multiple circulation zones are formed inside the tank. In the lower region, there are two relatively large circulation loops: fluid moves outward from the vicinity of the impeller blades, then downward along the tank wall, and finally returns to the central region. The upper helical ribbon creates a relatively stable axial circulation structure with several consecutive small loops. The velocity near the tank center in the middle region is low, indicating weaker local mixing intensity, which may lead to insufficient mixing in this area. The advantage of this configuration is that it provides a large overall circulation range and significant fluid exchange between the upper and lower regions. The pitched-blade turbine also helps better disperse gas entering at the bottom, enhancing gas distribution.

ISSN: 2472-3703 DOI: 10.6911/WSRJ.202603_12(3).0006

Figure 4 (b) shows that near the lower double helical ribbon impeller of Scheme 2, distinct medium-to-high velocity regions are formed. The helical ribbon directly acts on the fluid near the tank bottom, resulting in significantly increased velocity in the lower region. A noticeable axial velocity band appears at the bottom, which lifts the solid particles deposited at the bottom and moves them upward along the axial direction under the impeller's action. Near the upper pitched-blade turbine impeller, local high-velocity zones are also observed, but their extent is relatively small. As shown in Figure 4 (e), strong circulation forms in the bottom region. Fluid rises from the central bottom area, forming multiple local loops near the impeller blades and tank wall, which enhances the mixing intensity of solid particles. The upper region forms local circulation under the turbine impeller, but the overall circulation intensity is weaker than in the bottom region. This configuration is favorable for solid dispersion because the solids initially settle at the tank bottom, where the helical ribbon is located. The ribbon can directly draw the bottom solids into the main circulation, promoting particle suspension. The upper turbine impeller generates radial jets during rotation, producing strong local disturbances that enhance mixing in the mid-to-upper regions. Compared with Scheme 1, this structure more effectively drives the bottom fluid, making it more advantageous for bottom particles to participate in the overall circulation.

For Scheme 3, the double-layer turbine impeller configuration, the velocity contour in Figure 4 (c) and the vector plot in Figure 4 (f) show that high-velocity regions are mainly concentrated near the two turbine impellers. Velocities are significantly lower in areas away from the blades. The velocity vector plot indicates that two large circulation regions form inside the reactor, each surrounding a turbine impeller. The turbine impellers are typical radial-flow impellers, primarily driving fluid motion in the radial direction. This configuration generates strong local shear near the impellers. However, its axial transport capability is relatively weak, resulting in limited fluid exchange between the upper and lower regions. Consequently, relatively independent circulation zones are likely to form within the tank.

ISSN: 2472-3703 DOI: 10.6911/WSRJ.202603_12(3).0006

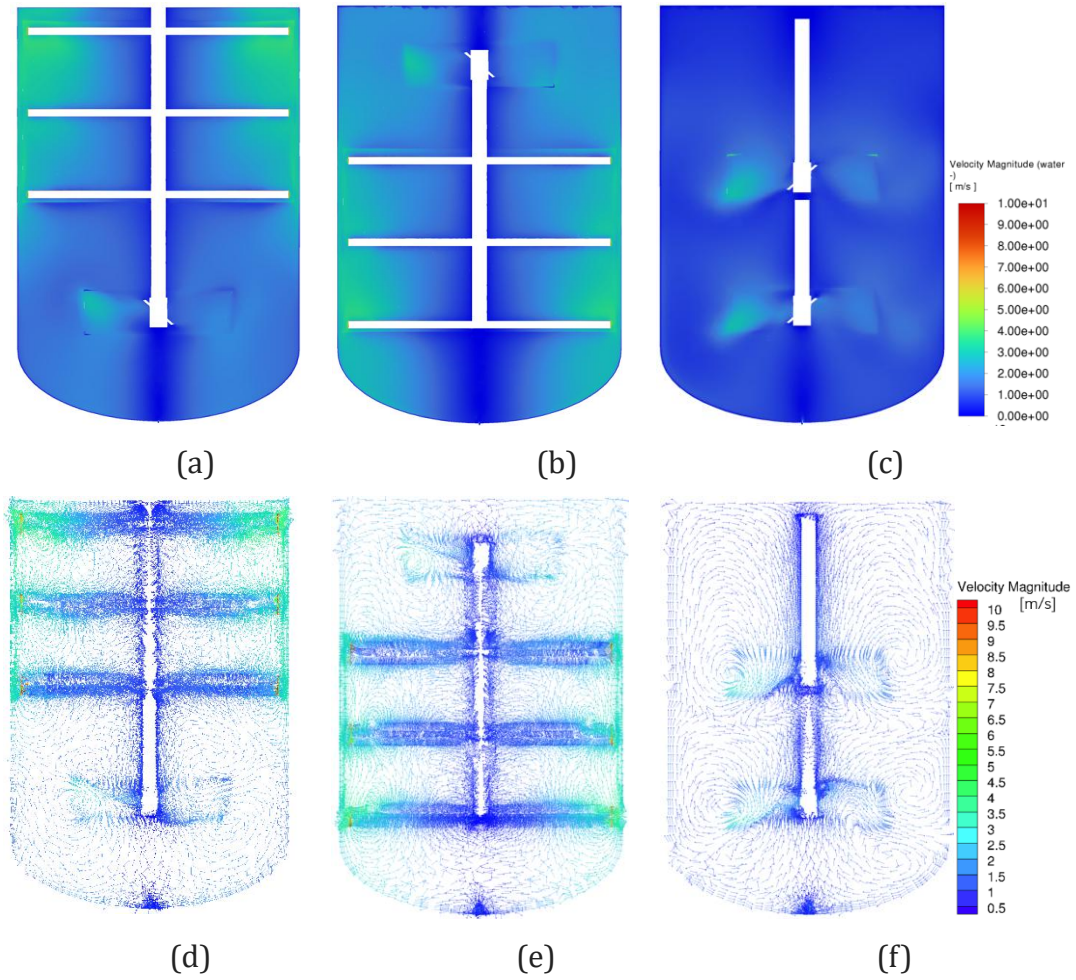


Figure 4. Velocity contour and vector plot on the vertical plane

Figure 5 shows the liquid velocity distribution at the Z = 1800 mm cross-section of the reactor for the three configurations. Overall, the velocity distribution curves of the three schemes exhibit a similar trend. The liquid velocity reaches higher values near the reactor walls, while it significantly decreases in the central region, resulting in a profile with high velocities at the sides and low in the middle. This indicates that at this height, the fluid mainly forms strong circulation along the wall regions, whereas the central region experiences relatively weaker flow intensity.

Comparing the different configurations, it can be seen that Configurations 1 and 2 exhibit higher overall velocities. In the side regions, the maximum velocity of Configuration 1 reaches nearly 3.2 m/s, while Configuration 2 shows a velocity distribution similar to Configuration 1, though slightly lower in the central region. This indicates that both configurations can generate strong radial flow at this cross-section, promoting circulation within the plane. In contrast, Configuration 3 shows significantly lower overall velocities. In the side regions, its maximum velocity is around 2.0 m/s, and the curve varies more gently. This suggests that the flow intensity generated by Configuration 3 at this height is weaker, and its ability to drive fluid circulation is relatively limited.

Combining the previous flow field and turbulence analysis results, it can be seen that Configurations 1 and 2 generate strong circulation and higher turbulence intensity within the reactor, thus maintaining relatively high fluid velocities at this cross-section. Although Configuration 3 has lower energy consumption, its overall flow intensity is comparatively weak, resulting in significantly lower velocities in the upper regions. These findings are generally consistent with the earlier analyses of gas distribution and turbulence intensity.

ISSN: 2472-3703 DOI: 10.6911/WSRJ.202603_12(3).0006

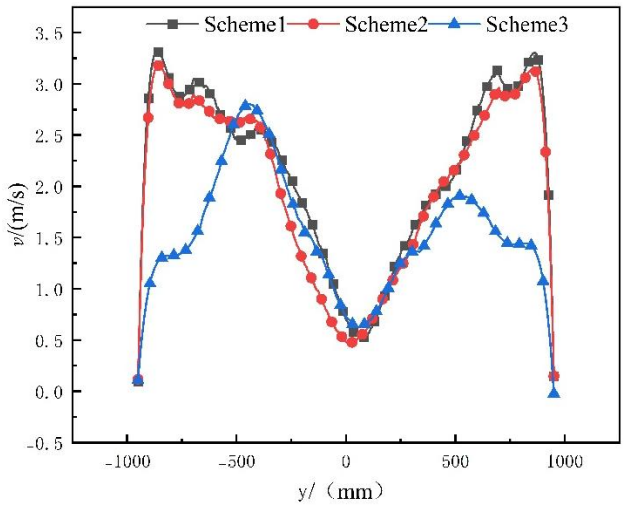


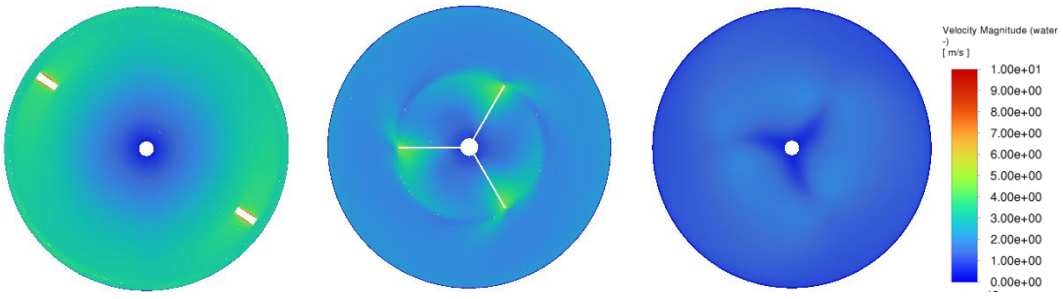
Figure 5. Liquid velocity of the three schemes at Z = 1800 mm

4.2. Analysis of the Solid Phase State

From the velocity distribution at the Z = 1800 mm section, the flow behavior in the upper region can be further observed. In Scheme 1, the section still maintains a relatively uniform velocity distribution, with velocities at the blade edges significantly higher than those at the blade centers. Compared with the other two schemes, the overall velocity is noticeably higher. As shown in Figure 6 (a) and Figure 7 (a), the circulation generated by the lower blades is transmitted to the upper region, forming a complete axial circulation throughout the reactor. This structure facilitates the overall transport of the gas and solid phases within the reactor.

In Scheme 2, Figure 6 (b) and Figure 7 (b) show that a distinct rotational flow structure forms at the section, and the blade-induced flow creates a large velocity gradient in the central region. This structure enhances fluid exchange in the center and provides advantages for gas dispersion and local mixing. However, there are still low-velocity zones near the tank wall, indicating that overall uniformity could be further improved.

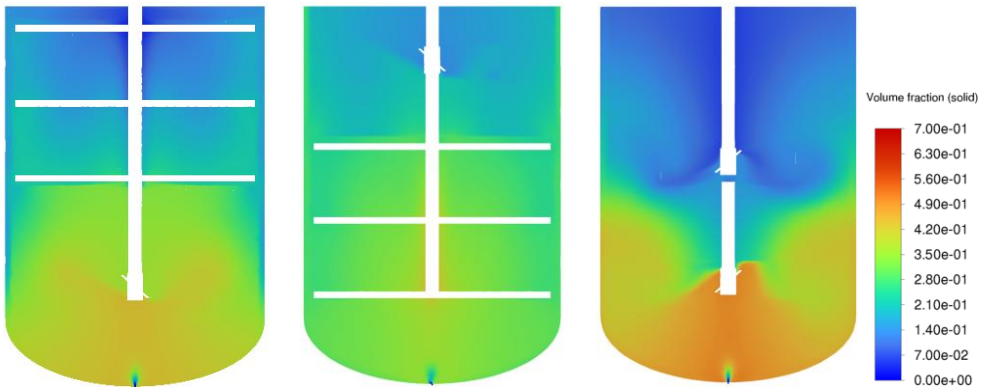
For Scheme 3, as shown in Figure 6 (c) and Figure 7 (c), the section is dominated by low-velocity regions, with only localized increases along the blade rotation direction, and the solid-phase concentration is lower compared with the other two schemes. This indicates that the flow induced by this blade type is primarily confined to local regions and struggles to form a macroscopic circulation throughout the reactor, resulting in weaker fluid renewal in the upper area.



(a) (b) (c)

Figure 6. Velocity distribution at the Z = 1800 mm section

ISSN: 2472-3703 DOI: 10.6911/WSRJ.202603_12(3).0006



(a) (b) (c)

Figure 7. Solid phase distribution cloud at the vertical section

4.3. Gas Phase Analysis

Figure 8 shows the average volume fraction distribution of CO_2 for the three impeller types at 20 s. Overall, all three configurations exhibit a similar trend in the axial direction, with higher gas fractions in the lower region of the reactor, gradually decreasing with increasing height.

Comparison of the three configurations shows that Scheme 2 has the highest overall gas volume fraction and a broader distribution range. This indicates that Scheme 2 can introduce more gas into the system and promote axial gas dispersion, resulting in a more uniform gas distribution. In contrast, Schemes 1 and 3 exhibit similar distribution trends, with gas mainly concentrated near the impellers and a rapid decrease in volume fraction in the upper regions, indicating weaker upward transport of gas beyond the impellers.

Overall, Scheme 2 exhibits the strongest gas dispersion and axial transport capabilities, while Schemes 1 and 3 have a comparatively weaker effect on the upper regions of the reactor.

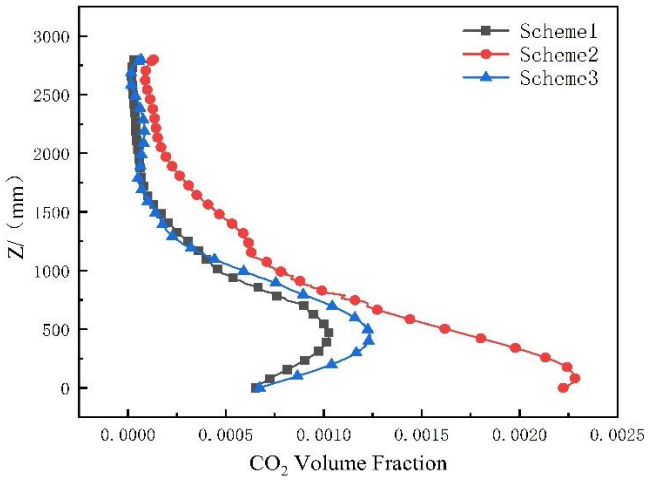


Figure 8. Average gas volume fraction for the three impeller types

5. CONCLUSION

From the comprehensive analysis of flow velocity, solid volume fraction, and gas volume fraction, it can be seen that different impeller combinations have a significant impact on the internal flow and multiphase distribution of the reactor. In terms of the flow field, Scheme 1 and 2 can form strong circulation with higher fluid velocities and larger flow coverage, while Scheme 3 has relatively weaker overall flow intensity. Regarding solid phase distribution, Scheme 1 and 2 better promote the suspension and dispersion of solid particles, resulting in a more uniform solid distribution within the reactor, whereas Scheme 3 has the weakest ability to transport

ISSN: 2472-3703 DOI: 10.6911/WSRJ.202603_12(3).0006

solid particles. For gas phase distribution, Scheme 2 can more effectively transport the gas from the bottom to the middle and upper regions of the reactor, achieving a larger and more uniform gas distribution, while in Scheme 1 and 3, the gas is mainly concentrated near the impellers, with a relatively lower gas fraction in the upper region.

Overall, Scheme 2 demonstrates more pronounced performance in flow intensity, solid suspension, and gas dispersion, providing better enhancement of the mixing process within the reactor.

REFERENCES

[1] Seifritz W J N. CO2 disposal by means of silicates. 1990, 345(6275): 486-.

[2] Back J, Zevenhoven R, Fagerlund J, et al. Mineral carbonation using mine tailings-a strategic overview of potential and opportunities; proceedings of the Proceedings of the 16th Greenhouse Gas Control Technologies Conference (GHGT-16), F, 2022.

[3] G. Wu, Y.F. Liu, L.P. Cui, et al. Comparison of the Carbonation Reaction Properties of Typical Industrial Solid Wastes & Acta Petrolei Sinica (Petroleum Processing Section). 2020, 36(01): 169-78.

[4] Z.H. Wang, S.Su, Z.J. Yi, et al. Research progress of CO2mineralization and integratedabsorption-mineralization (IAM) method & Chemical Industry and Engineering Progress. 2021, 40(04): 2318-27.

[5] W.LI, Y. Huang, WANG T, et al. Preparation of calcium carbonate nanoparticles from waste carbide slag based on CO2 mineralization. 2022, 363: 132463.

[6] Ragipani R, Sreenivasan K, Anes R P, et al. Direct air capture and sequestration of CO2 by accelerated indirect aqueous mineral carbonation under ambient conditions. 2022, 10(24): 7852-61.

[7] X.F. Zhen, Y. Huang, D. Xu, et al. Alkaline solid waste CO2 mineralization utilization technologyengineering application progress & Clean Coal Technology. 1-14.

[8] X. Xi, S.X. Sang, S.Q. Liu. Progress in research of CO2 fixation and sequestration by coal mine solid wastemineralization and co-disposal of pollution and carbon reduction & Journal of China Coal Society. 2024, 49(08): 3619-34.

[9] B.B. Zhang, H.M. Wang, S.H. Zeng, et al. Current status and outlook of carbon dioxide mineral carbonationtechnologies & Chemical Industry and Engineering Progress. 2012, 31(09): 2075-83.

[10] O'connor W K, Dahlin D C, RUSH G, et al. Carbon dioxide sequestration by direct mineral carbonation: process mineralogy of feed and products. 2002, 19(2): 95-101.

[11] J X Xu, H Wang, Wang J J, et al. CFD Simulation of Mixing Effects in Gas-Liquid-Solid Stirred Reactor. 2012, 383: 5778-84.

[12] Brucato A, Ciofalo M, Grisafi F, et al. Numerical prediction of flow fields in baffled stirred vessels: A comparison of alternative modelling approaches. 1998, 53(21): 3653-84.

[13] G.Z. Zhou. Numerical simulation of mixingprocess in a stirred tank.; Beijing University of Chemical Technology, 2002.

[14] Navier C-L J C C-G P, France. Navier stokes equation. 1838.

[15] Van Gool W J E. Thermodynamic aspects of energy conservation. 1980, 5(8-9): 783-92.

[16] Ranade V V. Computational flow modeling for chemical reactor engineering. Elsevier, 2001.